ceramic implants in bone tumor surgery. A long-term follow-up study. *J. Bone Joint Surg. Br.* **86**, 719–725. (doi:10.1302/0301-620X.86B5.14242)

Miyamoto, S., Takaoka, K., Okada, T., Yoshikawa, H., Hashimoto, J., Suzuki, S. & Ono, K. 1993 Polylactic acid-polyethylene glycol block copolymer: a new biodegradable synthetic carrier for bone morphogenetic protein. *Clin. Orthop.* **294**, 333–343.

Myoui, A., Tamai, N., Nishikawa, M., Araki, N., Nakase, T., Akita, S. & Yoshikawa, H. 2004 Three-dimensionally engineered hydroxyapatite ceramics with interconnected pores as a bone substitute and tissue engineering scaffold. In *Biomaterials in orthopedics* (eds M. J. Yaszemski, D. J. Trantolo, K. U. Lewandrowski, V. Hasirci, D. E. Altobelli & D. L. Wise), pp. 287–300. New York, NY: Marcel Dekker.

Nakasa, T., Ishida, O., Sunagawa, T., Nakamae, A., Yasunaga, Y., Agung, M. & Ochi, M. 2005 Prefabrication of vascularized bone graft using a combination of fibroblast growth factor-2 and vascular bundle implantation into a novel interconnected porous calcium hydroxyapatite ceramic. *J. Biomed. Mater. Res.* **75A**, 350–355. (doi:10.1002/jbm.a.30435)

Nakase, T. & Yoshikawa, H. 2006 Potential roles of bone morphogenetic proteins (BMPs) in skeletal repair and regeneration. *J. Bone Mineral Metab.* **24**, 425–433. (doi:10.1007/s00774-006-0718-8)

Nishikawa, M. & Ohgushi, H. 2004 Calcium phosphate ceramics in Japan. In *Biomaterials in orthopedics* (eds M. J. Yaszemski, D. J. Trantolo, K. U. Lewandrowski, V. Hasirci, D. E. Altobelli & D. L. Wise), pp. 425–436. New York, NY: Marcel Dekker.

Nishikawa, M., Myoui, A., Ohgushi, H., Ikeuchi, M., Tamai, N. & Yoshikawa, H. 2004 Bone tissue engineering using novel interconnected porous hydroxyapatite ceramics combined with marrow mesenchymal cells: quantitative and three-dimensional image analysis. *Cell Transplant.* **13**, 367–376. (doi:10.3727/000000004783983819)

Nishikawa, M., Ohgushi, H., Tamai, N., Osuga, K., Uemura, M., Yoshikawa, H. & Myoui, A. 2005 The effect of simulated microgravity by three-dimensional clinostat on bone tissue engineering. *Cell Transplant.* **14**, 829–835. (doi:10.3727/000000005783982477)

Ohgushi, H. & Caplan, A. I. 1999 Stem cell technology and bioceramics: from cell to gene engineering. *J. Biomed. Mater. Res.* **48A**, 913–927. (doi:10.1002/(SICI)1097-4636(1999)48:6<913::AID-JBM22>3.0.CO;2-0)

Omae, H., Mochizuki, Y., Yokoya, S., Adachi, N. & Ochi, M. 2006 Effects of interconnecting porous structure of hydroxyapatite ceramics on interface between grafted tendon and ceramics. *J. Biomed. Mater. Res. A* **79**, 329–337. (doi:10.1002/jbm.a.30797)

Omae, H., Mochizuki, Y., Yokoya, S., Adachi, N. & Ochi, M. 2007 Augmentation of tendon attachment to porous ceramics by bone marrow stromal cells in a rabbit model. *Int. Orthop.* **31**, 353–358. (doi:10.1007/s00264-006-0194-8)

Prolo, D. J. & Rodrigo, J. J. 1985 Contemporary bone graft physiology and surgery. *Clin. Orthop.* **200**, 322–342. (doi:10.1097/00003086-198511000-00036)

Roy, T. D., Simon, J. L., Ricci, J. L., Rekow, E. D., Thompson, V. P. & Parsons, J. R. 2003 Performance of degradable composite bone repair products made via three-dimensional fabrication techniques. *J. Biomed. Mater. Res. A* **66**, 283–291. (doi:10.1002/jbm.a.10582)

Saito, N., Okada, T., Horiuchi, H., Murakami, N., Takahashi, J., Nawata, M., Ota, H., Miyamoto, S., Nozaki, K. & Takaoka, K. 2001 Biodegradable poly-D,L-lactic acid-polyethylene glycol block copolymers as a BMP delivery system for inducing bone. *J. Bone Joint Surg.* **83A**, S92–S98.

Sartoris, D. J., Gershuni, D. H., Akeson, W. H., Holmes, R. E. & Resnick, D. 1986 Coralline hydroxyapatite bone graft substitutes: preliminary report of radiographic evaluation. *Radiology* **159**, 133–137.

Shi, K., Hayashida, K., Hashimoto, J., Sugamoto, K., Kawai, H. & Yoshikawa, H. 2006 Hydroxyapatite augmentation for bone atrophy in total ankle replacement in rheumatoid arthritis. *J. Foot Ankle Surg.* **45**, 316–321. (doi:10.1053/j.jfas.2006.06.001)

Simon, J. L., Roy, T. D., Parsons, J. R., Rekow, E. D., Thompson, V. P., Kemnitzer, J. & Ricci, J. L. 2003 Engineered cellular response to scaffold architecture in a rabbit trephine defect. *J. Biomed. Mater. Res. A* **66**, 275–282. (doi:10.1002/jbm.a.10569)

Simon, J. L., Michna, S., Lewis, J. A., Rekow, E. D., Thompson, V. P., Smay, J. E., Yampolsky, A., Parsons, J. R. & Ricci, J. L. 2007 *In vivo* bone response to 3D periodic hydroxyapatite scaffolds assembled by direct ink writing. *J. Biomed. Mater. Res. A* **83**, 747–758. (doi:10.1002/jbm.a.31329)

Simon, J. L., Rekow, E. D., Thompson, V. P., Beam, H., Ricci, J. L. & Parsons, J. R. 2008 MicroCT analysis of hydroxyapatite bone repair scaffolds created via three-dimensional printing for evaluating the effects of scaffold architecture on bone ingrowth. *J. Biomed. Mater. Res. A* **85**, 371–377.

Steinkamp, J. A., Hansen, K. M. & Crissman, H. A. 1976 Flow microfluorometric and light-scatter measurement of nuclear and cytoplasmic size in mammalian cells. *J. Histochem. Cytochem.* **24**, 292–297.

Tamai, N., Myoui, A., Tomita, T., Nakase, T., Tanaka, J., Ochi, T. & Yoshikawa, H. 2002 Novel hydroxyapatite ceramics with an interconnective porous structure exhibit superior osteoconduction *in vivo*. *J. Biomed. Mater. Res.* **59A**, 110–117. (doi:10.1002/jbm.1222)

Tamai, N., Myoui, A., Hirao, M., Kaito, T., Ochi, T., Tanaka, J., Takaoka, K. & Yoshikawa, H. 2005 A new biotechnology for articular cartilage repair: subchondral implantation of a composite of interconnected porous hydroxyapatite, synthetic polymer (PLA/PEG), and bone morphogenetic protein-2 (rhBMP-2). *Osteoarthr. Cartil.* **13**, 405–417. (doi:10.1016/j.joca.2004.12.014)

Uchida, A., Nade, S. M., McCartney, E. R. & Ching, W. 1984 The use of ceramics for bone replacement. A comparative study of three different porous ceramics. *J. Bone Joint Surg. Br.* **66**, 269–275.

Uchida, A., Araki, N., Shinto, Y., Yoshikawa, H., Kurisaki, E. & Ono, K. 1990 The use of calcium hydroxyapatite ceramic in bone tumour surgery. *J. Bone Joint Surg. Br.* **72**, 298–302.

Wozney, J. M. & Rosen, V. 1998 Bone morphogenetic protein and bone morphogenetic protein gene family in bone formation and repair. *Clin. Orthop.* **346**, 26–37. (doi:10.1097/00003086-199801000-00006)

Yoshikawa, H. & Myoui, A. 2005 Bone tissue engineering with porous hydroxyapatite ceramics. *J. Artif. Organs* **8**, 131–136. (doi:10.1007/s10047-005-0292-1)

Yoshikawa, H. & Uchida, A. 1999 Clinical application of calcium hydroxyapatite ceramic in bone tumor surgery. In *Biomaterials and bioengineering handbook* (ed. D. L. Wise), pp. 433–455. New York, NY: Marcel Dekker.

Author Queries

JOB NUMBER: 20080425

JOURNAL: RSIF

Q1 The same acronym 'IP-CHA' has been provided for two different expansions 'interconnected porous HA' and 'Interconnected porous HA ceramics'. Please check and confirm the appropriate acronyms.

Q2 Please check the edit of 'as little as 3 per cent' to 'as low as 3 per cent' in the sentence 'Although allogeneic bone…'

Q3 Please confirm the edit of 'non-organic' to 'inorganic' in the sentence 'Therefore, many kinds of biomaterials…'

Q4 Please check the edit of the sentence 'The tumours were located…'

Q5 Please check the edit of 'repaired' to 'fixed' in the sentence 'All bone defects in groups treated…'

Q6 Please check the edit of 'cartilageous' to 'cartilaginous' in the sentence 'Our new strategy for articular cartilage…'

Q7 Please check the edit of 'as little as three weeks' to 'as early as three weeks' in the sentence 'Our new strategy for…'

Arch Orthop Trauma Surg
DOI 10.1007/s00402-008-0800-x

ORTHOPAEDIC SURGERY

Correction of severe wrist deformity following physeal arrest of the distal radius with the aid of a three-dimensional computer simulation

Tsuyoshi Murase · Kunihiro Oka · Hisao Moritomo · Akira Goto · Kazuomi Sugamoto · Hideki Yoshikawa

Received: 12 July 2008
© Springer-Verlag 2008

Abstract Growth arrest following physeal injury may result in severe limb deformity. We report a case of complex wrist deformity caused by injury to the distal radial physis resulting in radial shortening and abnormal inclination of the radial articular surface, which was successfully treated by gradual correction after computer simulation. The simulation enabled us to develop an appropriate operative plan by accurately calculating the axis of the three-dimensional (3D) deformity using computer bone models. In the simulative surgery with a full-size stereolithography bone model, an Ilizarov external fixator was applied to the radius such that its two hinges were located on the virtual axis of the deformity, which was reproduced in the actual surgery. This technique of 3D computer simulation is a useful alternative to plan accurate correction of complex limb deformities following growth arrest.

Keywords Computer simulation · Deformity correction · Gradual lengthening · Physeal arrest · Distal radius

Electronic supplementary material The online version of this article (doi:10.1007/s00402-008-0800-x) contains supplementary material, which is available to authorized users.

T. Murase (✉) · K. Oka · H. Moritomo · A. Goto · H. Yoshikawa
Department of Orthopaedic Surgery,
Osaka University Graduate School of Medicine,
2-2, Yamada-Oka, Suita, Osaka 565-0871, Japan
e-mail: tmurase-osk@umin.ac.jp

K. Sugamoto
Department of Orthopaedic Biomaterial Science,
Osaka University Graduate School of Medicine,
2-2, Yamada-Oka, Suita, Osaka 565-0871, Japan

Published online: 19 December 2008

Introduction

Growth arrest following physeal injury to the distal radius may result in complex wrist deformities such as radial shortening and abnormal inclination of the radial articular surface, and it has been a challenging therapeutic problem [4, 14, 28, 30]. Although several previous reports have recommended gradual correction by lengthening using an external fixator, it is not always easy to devise an appropriate preoperative plan for three-dimensionally complex periarticular deformities [2, 21]. On the other hand, recent advances in computed tomography (CT) and three-dimensional (3D) image processing technology have enabled us to precisely simulate 3D correction of such difficult deformities [3, 10]. We have suggested that, in 3D computer simulation, a screw displacement axis (SDA) of the deformed segment relative to the rest of the bone appropriately serves as a 3D deformity axis, enabling the deformity correction to be planned accordingly [11, 20, 27].

We report a case of severe wrist deformity following physeal arrest of the distal radius that was successfully treated by application of an Ilizarov external fixator using a unique preoperative simulation based on the 3D deformity axis, which was calculated using an original computer program [19].

Case presentation

A 7-year-old boy sustained a fracture of the left distal radius, and was treated conservatively with a cast, although the distal fragment was displaced and malunited. Two months after the initial injury, he underwent corrective osteotomy at the same hospital; however, wrist deformity gradually developed during the follow-up period. He was

Fig. 1 Radial deviation of the wrist was obvious, and the ulnar head projected

referred to our hospital at 12 years of age when he complained of the unsightly appearance of his wrist and restricted range of wrist motion.

At first presentation, radial deviation of the wrist, and prominence of the ulnar head were obvious (Fig. 1). The range of wrist flexion was restricted to 20°, although wrist extension and forearm rotation were not impaired. Radiographs showed significant deformity of the distal radius and considerable radial and dorsal tilt with shortening (Fig. 2). MRI revealed that >50% of the physis was closed.

In order to plan corrective surgery for this complex deformity of the distal radius, we attempted to simulate 3D correction of the deformity using a computer model of the bone. First, the entire forearm was scanned by CT (GE LightSpeed Ultra16; scan time 0.5 s, slice thickness 1.25 mm, 30 mA, 120 kV), and the digital data were transferred to a computer. The contours of the radius, and ulna were semi-automatically segmented using commercially available software (Virtual Place M®, Medical Imaging Laboratory, Tokyo, Japan) and surface models of the bones were constructed by applying a 3D surface generation of the bone's cortex using Marching Cubes algorithm [15]. The geometrical models of the forearm bones were then visualized using a VTK-based original computer program (Visualization TookKit; Kitware Inc., Clifton Park, NY).

The degree of deformity of the radius can be expressed in terms of the displacement of the distal radius compared with the proximal part. The displacement is usually described by six parameters that measure rotation around and translation along the x, y, and z axes in any coordinate system; however, it can also be simply expressed as rotation around and translation along a unique axis in a SDA system (Fig. 3) [11, 27]. In this case, the axis around which the distal radius moves into normal position was calculated using the computer program. Normal position was determined using the mirror image of the contralateral normal radius as a reference. Simulation results demonstrated that the radial shortening, and abnormal articular inclination could be corrected by simply rotating the distal part of the radius by 40° around the axis that runs 3 cm volar to the wrist joint and at an angle of 60° to the transverse line of the radius (Fig. 4; see also the Supplementary video).

To investigate the feasibility of computer planning, we performed a simulative surgery with a full-size stereolithography bone model (CMET Inc., Yokohama, Japan) that was constructed from the CT data. An Ilizarov external fixator consisting of two rings at an angle of 40° to each other was attached to the radius of the resin model. The distal ring was fixed to the distal part of the radius-model with Kirschner wires, and the proximal ring was fixed to the radial diaphysis. The rings were connected by three rods. Two hinges were set on the two open-sided rods and were located on the simulated axis (Fig. 5a). By lengthening only the closed-sided rod after radial osteotomy, the distal ring together with the distal segment of the radius rotated around the simulated axis. When the two rings became parallel with each other, the distal radius rotated by 40°, resulting in simultaneous correction of the radial shortening, and dorsoradial inclination of the articular surface (Fig. 5b, c).

The stereolithography model was sterilized and brought into the operating theater as a surgical guide (Fig. 6), and the actual operation was performed according to the simulation so that the two hinges were located on the simulated axis. Lengthening began 1 week after the operation and ended after 10 weeks. Gradual correction of the radius occurred uneventfully, and new callus was well formed at the osteotomy site (Fig. 7). The external fixator was removed 15 weeks postoperatively, when adequate maturation of the callus had been confirmed through plain radiographs. A plastic orthosis was applied for another week, and then an active range of motion exercise was initiated. The radial inclination, and volar tilt on radiographs were corrected, as expected from the preoperative simulation (Fig. 8), and the appearance markedly improved after surgery (Fig. 9). The postoperative wrist flexion/extension, and forearm pronation/supination ranges of motion were 60°/80° and 80°/80°, respectively. The distal radio-ulnar joint was stable and painless.

Fig. 2 **a** AP and **b** lateral radiographs showed shortening of the radius with marked radial and dorsal inclination of the articular surface

Twenty months after the operation, when the patient was 14 years of age, the ulnar variance had increased to 2 mm, but the configuration of the radial articular surface remained the same. The patient was satisfied with the appearance of the wrist and does not complain of any functional limitation in daily life.

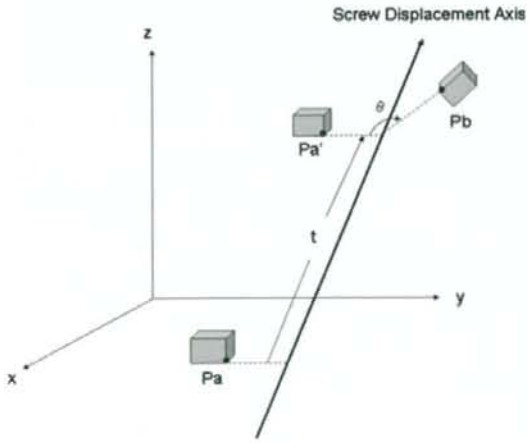

◀ **Fig. 3** General displacement of a rigid body in space can be described by a simultaneous translation along and a rotation about a unique axis. The figure shows the path of the rigid body from *Pa* to *Pb*. First, *Pa* moves to *Pa'* in parallel translation (t) along the unique axis (SDA) and then *Pa* moves to *Pb*, when rotated through θ° around the axis. Thus, the deformity can be expressed quite simply if one knows the SDA (axis) for the displacement of the distal radius in the current case

Discussion

Premature physeal closure following distal radial fracture in children occurs in about 4–7% of all cases [4, 14, 30] and sometimes results in severe deformity of the wrist [4, 14, 28, 30]. Patients with growth failure of more than 1 cm will have functional problems [4]. Therapeutic options include resection of the physeal bone bridge [12–14], corrective osteotomy [8, 14, 28, 31], epiphysiodesis of the distal ulna

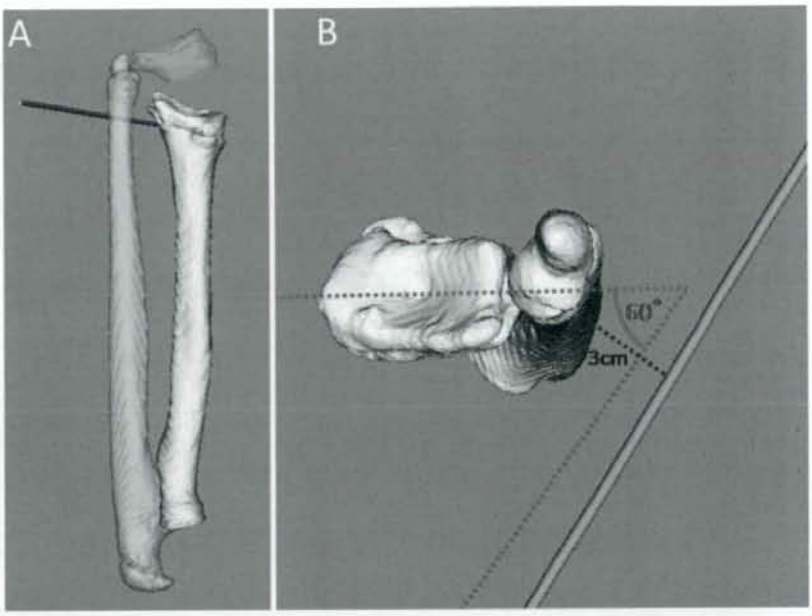

Fig. 4 Simulation results demonstrated that rotation around the axis (*pink*) by 40° brings the distal radius (*solid yellow*) into normal position (*semi-transparent yellow*) (**a**). The axis was 3 cm volar to the wrist joint and had an angle of 60° to the transverse line of the radius (**b**)

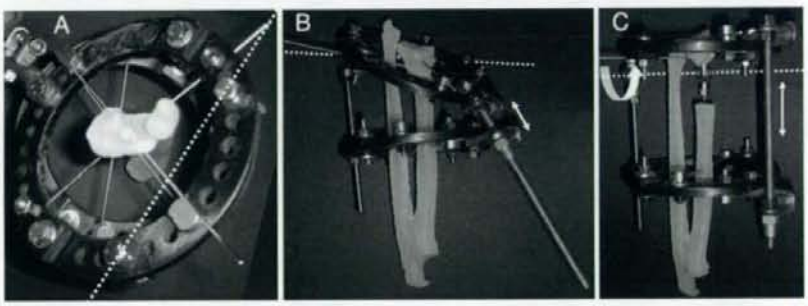

Fig. 5 An Ilizarov external fixator was attached to the full-sized stereolithography bone model. The line connecting the two hinges (*dotted line*) coincided with the simulated axis (**a**). By lengthening only one rod (*arrow*, **b** and **c**), the distal segment was rotated (*curved arrow*, **c**) around the simulated axis. Correction was completed when the two rings became parallel

[28], and radial lengthening [2, 17, 25]. Gradual lengthening and correction with distraction osteogenesis has been indicated for cases with severe deformities [2, 16]. For gradual correction, preoperative planning based on angular correction axis–center of rotation of angulation (ACA–CORA) obtained from radiographic measurements has been widely used [21, 23, 24, 29]. In cases of oblique plane deformity, the axis of deformity and the amount of angulation are calculated using trigonometric functions from measurement results of the anteroposterior, and lateral radiographs [22]. Despite the simplicity of using plain radiographs, accurate calculation of the position of and rotation around the axis of deformity can be difficult, especially in cases of severe periarticular deformity, in which the radiographic contour of the periarticular region is quite different from that of the contralateral normal bone.

With recent advances in CT scanning, however, 3D computer bone models are easily obtained and are becoming widely used in the planning of orthopaedic, and maxillofacial surgery [2, 9, 19, 26]. Use of 3D images to quantify the periarticular deformity enables gradual correction to be planned in a more straightforward and accurate manner. SDA technique, which was employed for the current preoperative simulation, is a method that expresses every body motion in terms of rotation around and translation along a unique axis [11, 27], and has been generally used to iden-

Fig. 6 The external fixator was set up before surgery, and the stereolithography model was sterilized and brought into the operating theater

tify the axis of motion of a joint in biomechanical studies [1, 5]. In several previous studies, the spatial position of the joint axis was calculated using 3D geometrical bone models constructed from CT or MRI data in different joint positions [6, 7, 18]. Consequently, the technique is quite familiar to biomechanical researchers who study joint kinematics. Our findings suggest that the axis of deformity in 3D planning for gradual correction could be determined using the SDA technique, because the deformity is regarded as a motion of the deformed segment relative to the rest of the bone, and we have developed an original computer program that enables us to easily calculate the position of and rotational amount around the axis of deformity by handling 3D bone models [19, 20].

The advantage of our computer simulation approach is its ability to make a very accurate operative plan by calculating the axis of deformity using CT bone models and by presenting it on a 3D viewer. By moving the displaced segment to the normal position with the computer mouse, the operator can have the program instantaneously calculate the 3D axis of deformity and the rotational and translational parameters. The operator can also observe the exact location of the axis from various angles using the 3D viewer. Another advantage of the method is its ability to build real-size mock-ups using the computer data. A stereolithography model is not always necessary for the operation, but in our case we found it useful as a means of confirming the feasibility of the preoperative simulation and to prepare the external fixator properly. The computer program used here

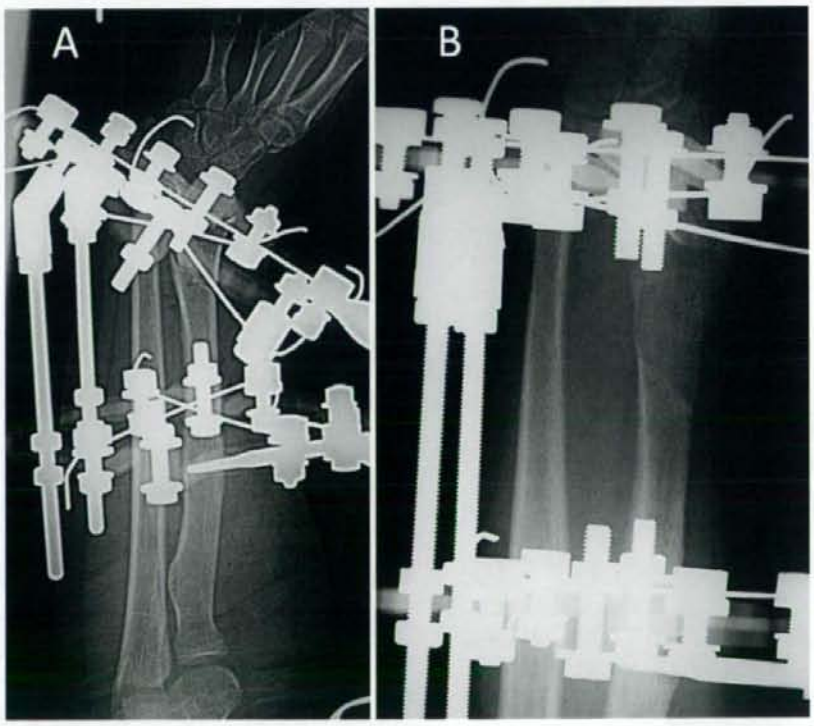

Fig. 7 Lengthening started 1 week after the operation (**a**) and lasted 10 weeks (**b**)

Fig. 8 **a**, **b** Shortening and articular inclination were well corrected, as predicted by the preoperative simulation

Fig. 9 The appearance was markedly improved after removal of the fixator

is available only in our institution at this stage; however, we are planning to distribute it. The time required for the preoperative simulation was 2 h. The cost of CT scanning and stereolithography modeling may be another drawback. We think, however, that these shortcomings will be overcome with advances in technology and could well be offset by the advantages mentioned above. We believe that our technique of computer simulation is useful in planning corrective surgery for severe limb deformity and hope that it will become the norm in near future to plan such surgeries.

Acknowledgments One of the authors (T.M.) has received a grant from Japan Science and Technology Agency. The authors thank Ryoji Nakao, computer programmer, Department of Orthopaedic Surgery, Osaka University Graduate School of Medicine for his contributions to this study.

References

1. An KN, Chao EY (1984) Kinematic analysis of human movement. Ann Biomed Eng 12:585–597. doi:10.1007/BF02371451
2. Aston JW Jr, Henley MB (1989) Physeal growth arrest of the distal radius treated by the Ilizarov technique. Report of a case. Orthop Rev 18:813–816
3. Athwal GS, Ellis RE, Small CF et al (2003) Computer-assisted distal radius osteotomy. J Hand Surg (Am) 28:951–958. doi:10.1016/S0363-5023(03)00375-7
4. Cannata G, De Maio F, Mancini F et al (2003) Physeal fractures of the distal radius and ulna: long-term prognosis. J Orthop Trauma 17:172–180. doi:10.1097/00005131-200303000-00002
5. Duck TR, Dunning CE, Armstrong AD et al (2003) Application of screw displacement axes to quantify elbow instability. Clin Biomech (Bristol, Avon) 18:303–310. doi:10.1016/S0268-0033(03)00021-4
6. Fischer KJ, Manson TT, Pfaeffle HJ et al (2001) A method for measuring joint kinematics designed for accurate registration of kinematic data to models constructed from CT data. J Biomech 34:377–383. doi:10.1016/S0021-9290(00)00195-0
7. Goto A, Moritomo H, Murase T et al (2004) In vivo elbow biomechanical analysis during flexion: three-dimensional motion analysis using magnetic resonance imaging. J Shoulder Elbow Surg 13:441–447
8. Hove LM, Engesaeter LB (1997) Corrective osteotomies after injuries of the distal radial physis in children. J Hand Surg [Br] 22:699–704. doi:10.1016/S0266-7681(97)80428-7
9. Jupiter JB, Ruder J, Roth DA (1992) Computer-generated bone models in the planning of osteotomy of multidirectional distal radius malunions. J Hand Surg [Am] 17:406–415. doi:10.1016/0363-5023(92)90340-U
10. Kanlic EM, Delarosa F, Pirela-Cruz M (2006) Computer assisted orthopaedic surgery—CAOS. Bosn J Basic Med Sci 6:7–13
11. Kinzel GL, Hall AS Jr, Hillberry BM (1972) Measurement of the total motion between two body segments. I. Analytical development. J Biomech 5:93–105. doi:10.1016/0021-9290(72)90022-X
12. Langenskiold A (1981) Surgical treatment of partial closure of the growth plate. J Pediatr Orthop 1:3–11
13. Langenskiold A, Osterman K (1979) Surgical treatment of partial closure of the epiphysial plate. Reconstr Surg Traumatol 17:48–64
14. Lee BS, Esterhai JL Jr, Das M (1984) Fracture of the distal radial epiphysis. Characteristics and surgical treatment of premature, posttraumatic epiphyseal closure. Clin Orthop Relat Res 185:90–96
15. Lorensen WE, Cline HE (1987) Marching cubes: a high resolution 3D surface construction algorithm. Comput Graph 21:163–169. doi:10.1145/37402.37422
16. Matsubara H, Tsuchiya H, Kabata T et al (2008) Deformity correction for vitamin D-resistant hypophosphatemic rickets of adults. Arch Orthop Trauma Surg 128:1137–1143. doi:10.1007/s00402-007-0548-8
17. Meier R, Prommersberger KJ, van Griensven M et al (2004) Surgical correction of deformities of the distal radius due to fractures in pediatric patients. Arch Orthop Trauma Surg 124:1–9. doi:10.1007/s00402-003-0585-x
18. Moritomo H, Murase T, Goto A et al (2006) In vivo three-dimensional kinematics of the midcarpal joint of the wrist. J Bone Joint Surg Am 88:611–621
19. Murase T, Moritomo H, Goto A et al (2005) Does three-dimensional computer simulation improve results of scaphoid nonunion surgery? Clin Orthop Relat Res 434:143–150
20. Murase T, Oka K, Moritomo H et al (2008) Three-dimensional corrective osteotomy of malunited fractures of the upper extremity with use of a computer simulation system. J Bone Joint Surg Am 90:2375–2389
21. Nakase T, Yasui N, Kawabata H et al (2007) Correction of deformity and shortening due to post traumatic epiphyseal arrest by distraction osteogenesis. Arch Orthop Trauma Surg 127:659–663. doi:10.1007/s00402-007-0339-2
22. Paley D (2002) Oblique plane deformities. In: Paley D (ed) Principles of deformity correction. Springer, Berlin, pp 175–194
23. Paley D, Tetsworth K (1992) Mechanical axis deviation of the lower limbs. Preoperative planning of multiapical frontal plane angular and bowing deformities of the femur and tibia. Clin Orthop Relat Res 280:65–71
24. Rozbruch SR, Paley D, Bhave A et al (2005) Ilizarov hip reconstruction for the late sequelae of infantile hip infection. J Bone Joint Surg Am 87:1007–1018. doi:10.2106/JBJS.C.00713
25. Sabharwal S (2004) Treatment of traumatic radial clubhand deformity with bone loss using the Ilizarov apparatus. Clin Orthop Relat Res 424:143–148. doi:10.1097/01.blo.0000128284.13331.c5
26. Shimizu T, Fujioka F, Gomyo H et al (2003) Three-dimensional starch model for simulation of corrective osteotomy for a complex bone deformity: a case report. Foot Ankle Int 24:364–367
27. Spoor CW, Veldpaus FE (1980) Rigid body motion calculated from spatial co-ordinates of markers. J Biomech 13:391–393. doi:10.1016/0021-9290(80)90020-2
28. Tang CW, Kay RM, Skaggs DL (2002) Growth arrest of the distal radius following a metaphyseal fracture: case report and review of the literature. J Pediatr Orthop B 11:89–92. doi:10.1097/00009957-200201000-00015
29. Waanders NA, Herzenberg JE (1992) The theoretical application of inclined hinges with the Ilizarov external fixator for simultaneous angulation and rotation correction. Bull Hosp Jt Dis 52:27–35
30. Waters PM, Mih AD (2005) Distal radius and ulna fractures. In: Beaty JH, Kasser JR (eds) Fractures in children, 6th edn. Lippincott, Philadelphia, pp 337–398
31. Zehntner MK, Jakob RP, McGanity PL (1990) Growth disturbance of the distal radial epiphysis after trauma: operative treatment by corrective radial osteotomy. J Pediatr Orthop 10:411–415

J Shoulder Elbow Surg (2009) 18, 33-37

ELSEVIER

JOURNAL OF SHOULDER AND ELBOW SURGERY

www.elsevier.com/locate/ymse

Morphologic analysis of the medullary canal in rheumatoid elbows

Akira Goto, MD, PhD[a,*], Tsuyoshi Murase, MD, PhD[a], Jun Hashimoto, MD, PhD[a], Kunihiro Oka, MD, PhD[a], Hideki Yoshikawa, MD, PhD[a], Kazuomi Sugamoto, MD, PhD[b]

[a]*Department of Orthopaedic Surgery, Osaka University Graduate School of Medicine, Suita, Osaka, Japan*
[b]*Department of Orthopaedic Biomaterial Science, Osaka University Graduate School of Medicine, Suita, Osaka, Japan*

Summary Total elbow arthroplasty is a standard approach for patients with arthritic elbows. To design appropriate stems for elbow prostheses, it is important to understand the shape of the medullary canals. The purpose of this study was to evaluate the shape and size of the medullary canals from normal cadavers and rheumatoid arthritis patients. These canals were measured based on geometric constructions of the 3-dimensional bone models generated from computed tomography images. The cross-sectional area of the medullary canals in rheumatoid arthritis patients decreased near the elbow joint as a result of morphologic changes after a long-standing inflammatory reaction. When designing the press-fit component of the humerus, an increase in the width of the transverse diameter of the intramedullary stem could increase stability in the canal. In contrast, for the ulnar component, such morphologic changes would impose difficulty in placing the press-fit model despite an anatomically designed stem. Therefore, a cement technique would be required for improved stabilization of the ulnar component.
© 2009 Journal of Shoulder and Elbow Surgery Board of Trustees.

Rheumatoid arthritis (RA) is an inflammatory condition, typified by synovial proliferation, that can affect multiple joints, with elbow involvement being the most common in nearly half of RA cases.[12] Total elbow arthroplasty (TEA) in rheumatoid patients is now a widely accepted therapeutic alternative for advanced elbow destruction. The advantage of TEA over simple synovectomy is that it can reduce pain, improve the range of joint motion, and provide long-term pain relief. However, loosening of the implants is one of the major complications and a primary concern. Although the improvement in surgical technique and prosthetic design has led to increased success with TEA, high rates of humeral component loosening have been reported previously.[5,8,18,23,26] Stem design of the prosthesis is considered an important factor that influences loosening of the implant. Data on the geometry of the medullary canals of the distal humerus and proximal ulna should help to design stems for elbow prostheses, which could occupy the medullary cavity, increase its stability with regard to the bone, and decrease the rate of loosening. However, in these patients, it is difficult to evaluate the morphologic analysis appropriately, based only on plain radiographs. In addition, RA patients have shown a restricted range of motion of the elbow with occasional valgus deformity because of erosive changes. Therefore, with only an axial computed tomography (CT) scan, it is difficult to evaluate the morphology accurately. Recent advancements in computer technology have enabled us to determine the precise geometry of the medullary canals generated from the CT data. We have

*Reprint requests: Akira Goto, MD, PhD, Department of Orthopaedic Surgery, Osaka University Graduate School of Medicine, 2-2, Yamadaoka, Suita, Osaka 565-0871, Japan.
E-mail address: goto-akira@umin.ac.jp (A. Goto).

1058-2746/2009/$36.00 - see front matter © 2009 Journal of Shoulder and Elbow Surgery Board of Trustees.
doi:10.1016/j.jse.2008.07.002

constructed 3-dimensional (3D) bone models and resliced the medullary canal vertically along its longitudinal axis to obtain accurate measurements. The purpose of this study was to evaluate the geometry of the medullary canals of the distal humerus and proximal ulna using 3D bone models constructed from the CT data and to compare them between normal cadavers and RA patients.

Materials and methods

We studied the elbow joints of 16 seropositive rheumatoid patients, who were scheduled for TEA (15 women and 1 man; age range, 48-81 years; mean age, 60.6 years) and 20 cadaveric dry bones (10 humeri and 10 ulnae) (Natural Bone; Sawbones [A Division of Pacific Research Laboratories], Vashon, WA). The inclusion criteria for RA patients included RA of grade III to V based on the radiographic criteria of Larsen et al,[10] severe disabling pain, limitation of elbow function, and no previous surgical treatment. Of the patients, 9 (56.2%) had Larsen grade III RA, 4 (25%) had Larsen grade IV RA, and 3 (18.8%) had Larsen grade V RA. The right elbow was affected in 10 patients and the left elbow in 6.

Image acquisition

Morphologic analysis of the medullary canal was performed by use of CT scans. Image data of the elbows from RA patients and cadavers were obtained with a helical CT system (Light Speed Ultra16; GE Medical Systems, Waukesha, WI). We used a sequence with 120 kV, 100 mA, a 300-mm field of view, and a thickness of 0.625 mm on a contiguous slice with a pixel size of 0.39×0.39 mm. During CT scanning, the elbow joint was maximally extended with the forearm in a neutral position. Scan data were saved in DICOM (Digital Imaging and Communications in Medicine) format.

Three-dimensional bone models and measurement

Contours and medullary structures of each bone were semiautomatically segmented from CT images by use of the Virtual Place-M software program (Medical Imaging Laboratory, Tokyo, Japan). This software generated 3D surface bone models via the marching cubes technique,[13] based on which we constructed bone models of each humerus and ulna. A threshold for constructing these models is an important parameter for determining their accuracy. In this study, we used 150 Hounsfield units as an optimal threshold value.[21] The contours of the medullary canal were extracted semiautomatically, and the visualization and measurement of the geometric shape and size of each bone were obtained by use of a visualization software program developed in our laboratory. The accuracy of this computer-based measurement was reported to be 0.4 mm.[17]

We resliced the 3D surface bone models of the medullary canal vertically along the longitudinal axis of each canal and evaluated the change in medullary shape of the reconstructed cross section of the humeral medullary canal, from the proximal margin of the olecranon fossa, and for the ulna, from the tip of the coronoid process, at intervals of 1 cm. Then, we calculated the area, as well as the anteroposterior and transverse diameters, of each cross-sectional slice of the medulla of the humerus and the ulna.

Statistical analysis

Mann-Whitney U tests were performed for statistical differences between normal controls and RA patients. A difference with $P < .05$ was considered significant. This statistical analysis was conducted with the Statcel2 statistical analysis software package for personal computers (OMS Publishing, Saitama, Japan).

Results

Morphology of humerus

The cross-sectional shape of the humerus changed from a V shape to an equilateral triangle and then to ovoid in both RA patients and cadavers (Figure 1, *A*). The cross-sectional area particularly decreased at 0 cm above the olecranon fossa compared with the cadavers ($P < .05$). It also tended to decrease at a distance of 1 cm (Figure 2, *A*). Whereas the mean anteroposterior diameter was not significantly different between RA patients and controls, the mean transverse diameter was significantly decreased at 0 and 1 cm in the RA patients as compared with the controls ($P < .05$), as shown in Figures 2, *B*, and 2, *C*. In RA patients and cadavers, the cross-sectional areas were approximately 100 mm^2 at 2 cm and 80 mm^2 at 3 to 10 cm and then they increased gradually at 11 cm. The mean anteroposterior diameters of the humerus tended to increase gradually toward the diaphysis, whereas the transverse diameters gradually decreased.

Morphology of ulna

For the ulna, the shape changed from ovoid to triangular (Figure 1, *B*), and the cross-sectional area decreased at 0 and 1 cm distal to the coronoid process in the RA patients ($P < .05$) (Figure 3, *A*). In the ulna, both the mean anteroposterior and transverse diameters were significantly decreased at 0 and 1 cm, respectively, in the RA patients compared with the controls ($P < .05$) (Figures 3, *B*, and 3, *C*). This discrepancy between RA patients and cadavers was produced by the morphologic changes observed around the trochlear notch of the ulna. In both RA patients and cadavers, the cross-sectional areas were approximately 50 mm^2 at 3 cm and 20 mm^2 at 7 cm to 14 cm. Both the mean anteroposterior and transverse diameters of the ulna tended to decrease gradually toward the diaphysis.

Discussion

TEA can preserve, or even improve, the range of motion of the joints, eliminate pain, and provide adequate stability to the arthritic joint. One major concern regarding TEA is loosening of the implants. Although improvement of surgical technique and prosthetic design has led to

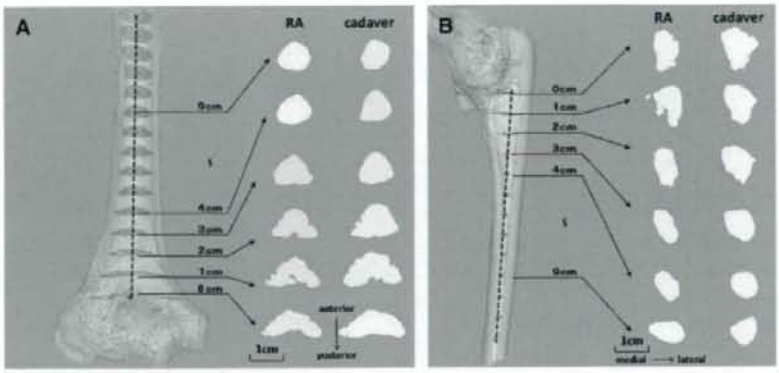

Figure 1 (**A**) Cross-sectional area of medullary canal of humerus. We evaluated the cross-sectional area from the proximal margin of the olecranon fossa at 1-cm intervals. The cross-sectional shape of the humerus changed from a V shape to an equilateral triangle and then to ovoid in both RA patients and cadavers. The cross-sectional area of RA has especially decreased at 0 cm above the olecranon fossa because of the morphologic change around the coronoid fossa, as compared with the cadavers ($P < .05$). (**B**) Cross-sectional area of medullary canal of ulna. The geometric shape of the cross-sectional area changed from ovoid to triangular. In the RA patients, the cross-sectional area decreased at 0 and 1 cm distal to the tip of the coronoid process because of the morphologic change around the trochlear notch of the ulna.

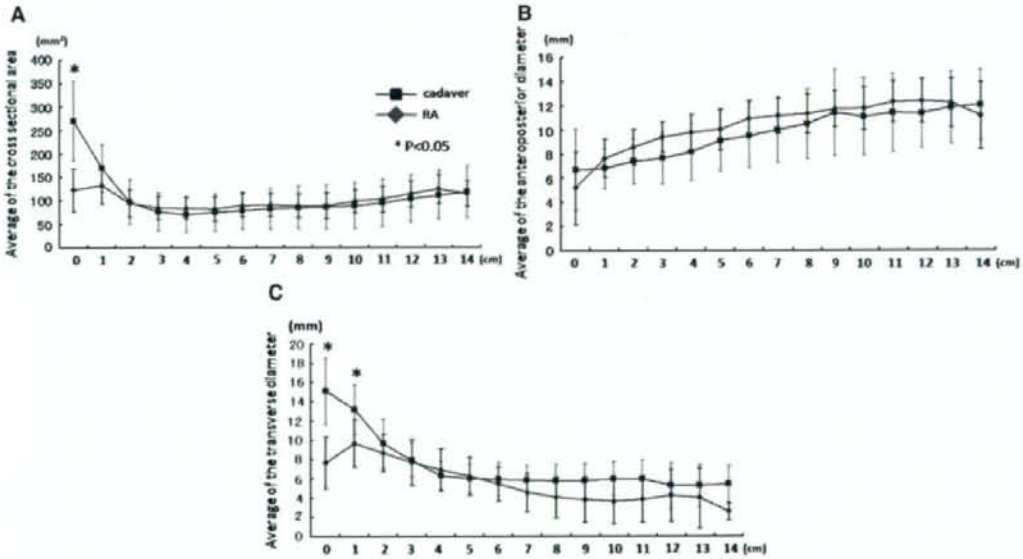

Figure 2 Measurement of medullary canal of humerus. (**A**) The mean cross-sectional area of the humerus is shown with SD error bars. *Asterisk*, A significant difference was found between the RA patients and cadavers ($P < .05$). (**B**) Mean anteroposterior diameters of cross section. (**C**) Mean transverse diameters of cross section.

increased longevity of TEA, the loosening rate is still higher when compared with total hip and knee arthroplasties.[5,6,8,18,19,23,26] In RA patients, van der Lugt et al[26,27] reported that the survival rate of the Souter-Strathclyde prosthesis, according to Kaplan-Meier analysis, was 77.4% after 10 years and 65.2% after 18 years. A high rate of aseptic loosening of the humeral component has been frequently described, whereas the success rate was found to be different among the types of TEA.[5,8,18,23,26] Although several authors postulate that the loosening was because of the micromovement, the reason for this phenomenon remains unclear.[2,24] Ikavalko et al[3,4] reported that the standard stem humeral component has better survivorship compared with the long-stemmed component.

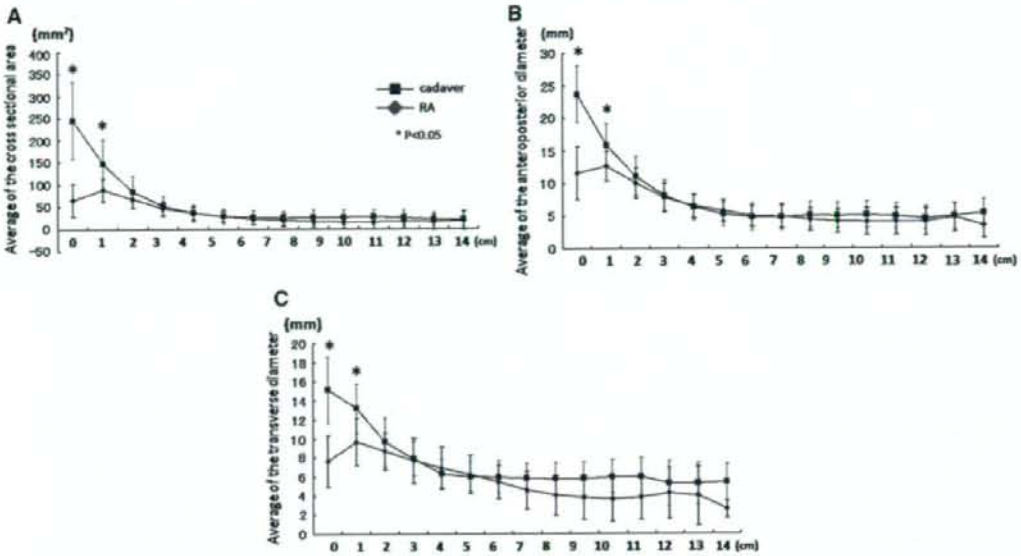

Figure 3 Measurement of medullary canal of ulna. (**A**) The mean cross-sectional area of the ulna is shown with SD error bars. *Asterisk*, A significant difference was found between the RA patients and cadavers ($P < .05$). (**B**) Mean anteroposterior diameters of cross section. (**C**) Mean transverse diameters of cross section.

We assumed that the morphologic change of periarticular inflammatory reaction from arthritis could possibly be one of the reasons for early aseptic loosening after TEA, as it can decrease the stability of the implant in regard to the bone. Therefore, it would be important to evaluate the morphologic change around the elbow joint in RA patients accurately. There have been several detailed studies of the geometry of the medullary canals based on radiographs.[7,11,20] However, it is quite difficult to quantify the extent of the bone loss correctly, based only on plane radiographs.

On the other hand, several authors believe that an anatomic, custom-designed femoral component of total hip arthroplasty is more likely to be effective than off-the-shelf components to achieve the optimal fit and fill the medullary canal.[14,15,28,29] The geometry of the medullary canals of the distal humerus and proximal ulna is considered important for the appropriate design of stems for the TEA prosthesis to increase its stability in the bone and decrease the rate of loosening. Our measurements were derived from 3D constructions of the medullary canal, based on the CT data obtained with a high-speed helical scanner. This allowed us to compare the morphology of the normal controls with the RA group accurately.

High loosening rates of the humeral component have been reported previously.[5,8,18,23,26] On the basis of the data obtained from this study, the anteroposterior diameters of the humerus have tended to increase toward the diaphysis whereas the transverse diameters have decreased (Figure 2, *B*). When considering the initial fixation of the press-fit uncemented stem of the humeral component in future prosthetic design, the width of the transverse diameter is considered more important than the anteroposterior diameter. Increasing the width of the transverse diameter of the intramedullary stem could increase the stability of the humeral component in the canal.

Several authors have noted that aseptic loosening and failure, because of loosening, occur more often with the ulnar component than with the humeral component and that the ulnar component is at high risk of loosening.[1,9,16,22,25] Furthermore, in RA patients, aseptic loosening of the ulnar component was found more often in uncemented ulnar components than in cemented ones. Our results showed that there is a significant morphologic change in the proximal ulnar medullary canal in the area from the coronoid process to 3 cm distally, where the stem of the prosthesis is expected to fit. This change in the morphology would make press fitting of the ulnar component into the canal quite difficult, even with an anatomically designed stem. We believe that the ulnar component would be better stabilized by a cement technique, especially in cases of severe morphologic change.

References

1. Brinkman JM, de Vos MJ, Eygendaal D. Failure mechanisms in uncemented Kudo type 5 elbow prosthesis in patients with rheumatoid arthritis: 7 of 49 ulnar components revised because of loosening after 2-10 years. Acta Orthop 2007;78:263-70.

2. Brunski BJ, Puelo DA, Nanci A. Biomaterials and biomechanics of oral and maxillofacial implants: current state and future developments. Int J Oral Maxillofac Implants 2000;15:15-46.
3. Ikavalko M, Belt EA, Kautiainen H, Lehto MU. Revisions for aseptic loosening in Souter-Strathclyde elbow arthroplasty: incidence of revisions of different components used in 522 consecutive cases. Acta Orthop Scand 2002;73:257-63.
4. Ikavalko M, Lehto MU, Repo A, Kautiainen H, Hamalainen M. The Souter-Strathclyde elbow arthroplasty. A clinical and radiological study of 525 consecutive cases. J Bone Joint Surg Br 2002;84:77-82.
5. Kasten MD, Skinner HB. Total elbow arthroplasty. An 18-year experience. Clin Orthop Relat Res 1993:177-88.
6. Khaw FM, Kirk LM, Gregg PJ. Survival analysis of cemented Press-Fit Condylar total knee arthroplasty. J Arthroplasty 2001;16:161-7.
7. Kitamura T, Hashimoto J, Murase T, Tomita T, Hattori T, Yoshikawa H, et al. Radiographic study of joint destruction patterns in the rheumatoid elbow. Clin Rheumatol 2007;26:515-9.
8. Kraay MJ, Figgie MP, Inglis AE, Wolfe SW, Ranawat CS. Primary semiconstrained total elbow arthroplasty. Survival analysis of 113 consecutive cases. J Bone Joint Surg Br 1994;76:636-40.
9. Landor I, Vavrik P, Jahoda D, Guttler K, Sosna A. Total elbow replacement with the Souter-Strathclyde prosthesis in rheumatoid arthritis. Long-term follow-up. J Bone Joint Surg Br 2006;88:1460-3.
10. Larsen A, Dale K, Eek M. Radiographic evaluation of rheumatoid arthritis and related conditions by standard reference films. Acta Radiol Diagn (Stockh) 1977;18:481-91.
11. Lehtinen JT, Kaarela K, Belt EA, Kauppi MJ, Skyttä E, Kuusela PP, et al. Radiographic joint space in rheumatoid elbow joints. A 15-year prospective follow-up study in 74 patients. Rheumatology (Oxford) 2001;40:1141-5.
12. Lehtinen JT, Kaarela K, Ikävalko M, Kauppi MJ, Belt EA, Kuusela PP, et al. Incidence of elbow involvement in rheumatoid arthritis. A 15 year endpoint study. J Rheumatol 2001;28:70-4.
13. Lorensen WE, Cline HE. Marching cubes: a high resolution 3-D surface construction algorithm. Computer Graphics 1987;21:163-9.
14. McCarthy JC, Bono JV, O'Donnell PJ. Custom and modular components in primary total hip replacement. Clin Orthop Relat Res 1997: 162-71.
15. Mulier JC, Mulier M, Brady LP, Steenhoudt H, Cauwe Y, Goossens M, et al. A new system to produce intraoperatively custom femoral prosthesis from measurements taken during the surgical procedure. Clin Orthop Relat Res 1989:97-112.
16. Potter D, Claydon P, Stanley D. Total elbow replacement using the Kudo prosthesis. Clinical and radiological review with five- to seven-year follow-up. J Bone Joint Surg Br 2003;85:354-7.
17. Robertson DD, Yuan J, Bigliani LU, Flatow EL, Yamaguchi K. Three-dimensional analysis of the proximal part of the humerus: relevance to arthroplasty. J Bone Joint Surg Am 2000;82:1594-602.
18. Rozing P. Souter-Strathclyde total elbow arthroplasty. J Bone Joint Surg Br 2000;82:1129-34.
19. Sathappan SS, Teicher ML, Capeci C, Yoon M, Wasserman BR, Jaffe WL. Clinical outcome of total hip arthroplasty using the normalized and proportionalized femoral stem with a minimum 20-year follow-up. J Arthroplasty 2007;22:356-62.
20. Stein H, Dickson RA, Bentley G. Rheumatoid arthritis of the elbow. Pattern of joint involvement, and results of synovectomy with excision of the radial head. Ann Rheum Dis 1975;34:403-8.
21. Sugano N, Sasama T, Sato Y, Nakajima Y, Nishii T, Yonenobu K, et al. Accuracy evaluation of surface-based registration methods in a computer navigation system for hip surgery performed through a posterolateral approach. Comput Aided Surg 2001;6:195-203.
22. Tanaka N, Kudo H, Iwano K, Sakahashi H, Sato E, Ishii S. Kudo total elbow arthroplasty in patients with rheumatoid arthritis: a long-term follow-up study. J Bone Joint Surg Am 2001;83:1506-13.
23. Trail IA, Nuttall D, Stanley JK. Survivorship and radiological analysis of the standard Souter-Strathclyde total elbow arthroplasty. J Bone Joint Surg Br 1999;81:80-4.
24. Valstar ER, Garling EH, Rozing PM. Micromotion of the Souter-Strathclyde total elbow prosthesis in patients with rheumatoid arthritis 21 elbows followed for 2 years. Acta Orthop Scand 2002; 73:264-72.
25. van der Heide HJ, de Vos MJ, Brinkman JM, Eygendaal D, van den Hoogen FH, de Waal Malefijt MC. Survivorship of the KUDO total elbow prosthesis-comparative study of cemented and uncemented ulnar components: 89 cases followed for an average of 6 years. Acta Orthop 2007;78:258-62.
26. van der Lugt JC, Geskus RB, Rozing PM. Primary Souter-Strathclyde total elbow prosthesis in rheumatoid arthritis. J Bone Joint Surg Am 2004;86:465-73.
27. van der Lugt JC, Rozing PM. Outcome of revision surgery for failed primary Souter-Strathclyde total elbow prosthesis. J Shoulder Elbow Surg 2006;15:208-14.
28. Wettstein M, Mouhsine E, Argenson JN, Rubin PJ, Aubaniac JM, Leyvraz PF. Three-dimensional computed cementless custom femoral stems in young patients: midterm followup. Clin Orthop Relat Res 2005:169-75.
29. Xenakis TA, Gelalis ID, Koukoubis TD, Soucacos PN, Vartziotis K, Kontoyiannis D, et al. Neglected congenital dislocation of the hip: role of computed tomography and computer-aided design for total hip arthroplasty. J Arthroplasty 1996;11:893-8.

Copyright © 2008 by The Journal of Bone and Joint Surgery, Incorporated

Three-Dimensional Corrective Osteotomy of Malunited Fractures of the Upper Extremity with Use of a Computer Simulation System

By Tsuyoshi Murase, MD, PhD, Kunihiro Oka, MD, PhD, Hisao Moritomo, MD, PhD, Akira Goto, MD, PhD, Hideki Yoshikawa, MD, PhD, and Kazuomi Sugamoto, MD, PhD

Investigation performed at the Department of Orthopaedic Surgery, Osaka University Graduate School of Medicine, Suita, Japan

Background: Three-dimensional anatomical correction is desirable for the treatment of a long-bone deformity of the upper extremity. We developed an original system, including a three-dimensional computer simulation program and a custom-made surgical device designed on the basis of simulation, to achieve accurate results. In this study, we investigated the clinical application of this system using a corrective osteotomy of malunited fractures of the upper extremity.

Methods: Twenty-two patients with a long-bone deformity of the upper extremity (four with a cubitus varus deformity, ten with a malunited forearm fracture, and eight with a malunited distal radial fracture) participated in this study. Three-dimensional computer models of the affected and contralateral, normal bones were constructed with use of data from computed tomography, and a deformity correction was simulated. A custom-made osteotomy template was designed and manufactured to reproduce the preoperative simulation during the actual surgery. When we performed the surgery, we placed the template on the bone surface, cut the bone through a slit on the template, and corrected the deformity as preoperatively simulated; this was followed by internal fixation. All patients underwent radiographic and clinical evaluations before surgery and at the time of the most recent follow-up.

Results: A corrective osteotomy was achieved as simulated in all patients. Osseous union occurred in all patients within six months. Regarding cubitus varus deformity, the humerus-elbow-wrist angle and the anterior tilt of the distal part of the humerus were an average of 2° and 28°, respectively, after surgery. Radiographically, the preoperative angular deformities were nearly nonexistent after surgery. All radiographic parameters for malunited distal radial fractures were normalized. The range of forearm rotation in patients with forearm malunion and the range of wrist flexion-extension in patients with a malunited distal radial fracture improved after surgery.

Conclusions: Corrective osteotomy for a malunited fracture of the upper extremity with use of computer simulation and a custom-designed osteotomy template can accurately correct the deformity and improve the clinical outcome.

Level of Evidence: Therapeutic Level IV. See Instructions to Authors for a complete description of levels of evidence.

Treatment of symptomatic osseous deformity of the extremity resulting from a malunited fracture is a challenge. Anatomically accurate correction is the key to obtaining good functional outcomes after corrective osteotomy, especially for the upper extremity[1-4]. However, conventional preoperative planning with two-dimensional plain radiographs has not always provided sufficient information to understand the complex three-dimensional deformity[5-9]. On the other hand, advances in computer technology, such as the development of a multidetector computed tomography scanner and rapid prototyping technology, have made accurate three-dimensional preoperative simulation possible[10-14]. To establish a reliable surgical treatment for malunited extremity fractures, we developed a simulation system consisting of a three-dimensional computer program and a custom-made osteotomy template that allows the reproduction of preoperative simulation during the actual

Disclosure: In support of their research for or preparation of this work, one or more of the authors received, in any one year, outside funding or grants in excess of $10,000 from the Japan Science and Technology Agency and the New Energy and Industrial Technology Development Organization. Neither they nor a member of their immediate families received payments or other benefits or a commitment or agreement to provide such benefits from a commercial entity. No commercial entity paid or directed, or agreed to pay or direct, any benefits to any research fund, foundation, division, center, clinical practice, or other charitable or nonprofit organization with which the authors, or a member of their immediate families, are affiliated or associated.

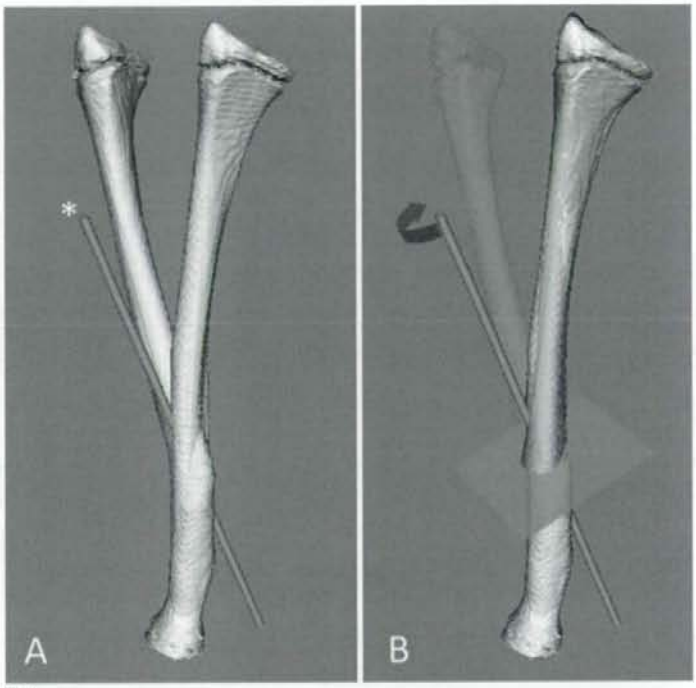

Fig. 1

Malunited radial fracture: By superimposing the malunited radius (yellow) with the mirror image of the contralateral, normal radius (white), we quantified the deformity of the distal part relative to the proximal part, which can be further defined in terms of rotation around and translation along a certain axis using the screw displacement axis technique[21-23]. When the translation is small, it can be simply regarded as the deformity axis (asterisk in A). Correction in this case is to be completed by performing a rotational osteotomy of 45° around the axis on the plane perpendicular to it (curved arrow in B).

surgery[15-17]. This system, despite some shortcomings, such as radiation exposure during computed tomography scanning and the time and expense necessary to develop the custom-made template, is expected to facilitate accurate anatomical correction with a simple osteotomy. The purpose of this study was to investigate the preliminary radiographic and clinical results of corrective osteotomy for malunited fractures of the upper extremity with use of this system.

Materials and Methods

Patients

Between January 2003 and October 2006, twenty-two consecutive patients with twenty-seven malunited fractures of the upper extremities underwent a corrective osteotomy with the use of preoperative simulation and a custom-made osteotomy template. All patients were followed for more than twelve months (range, fourteen to thirty-one months; mean, twenty-two months) (see Appendix). There were fourteen male and eight female patients with a mean age of thirty-two years (range, ten to seventy-two years) at the time of surgery. Our institutional review board approved this study. After informed consent was obtained from patients for participation in the study, a preoperative simulation, corrective osteotomy with use of the custom-made template, and physical and radiographic examinations were carried out.

Inclusion criteria included an osseous deformity of the radius, ulna, or humerus and an age of at least ten years at the time of surgery. Exclusion criteria included malunions of the hand and carpus, deformity with marked shortening that would require gradual lengthening, intra-articular involvement of the adjacent joint, and an age of less than ten years. Deformity of small bones and an age of less than ten years were considered exclusion criteria because the reliability of the operative technique with use of a surgical template for smaller bones had not been established and because active remodeling is expected in younger patients[18].

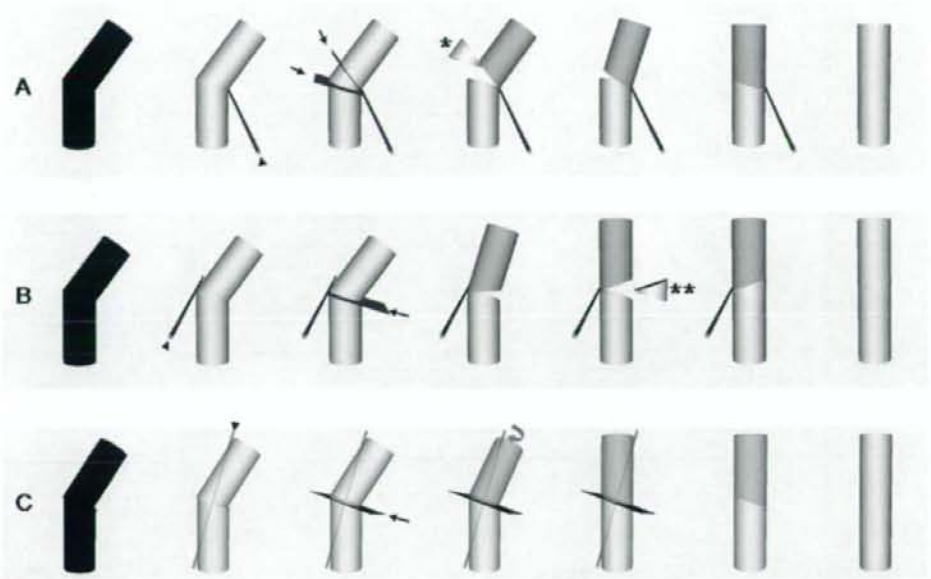

Fig. 2

The bent cylinders represent the deformed bones. Different deformities can show a similar silhouette (the left figures of A, B, and C). The three-dimensional relationship between the bone and the deformity axis (arrowhead of each figure) suggests the most appropriate method of correction. When the axis runs along the concave side of the deformity, a closing osteotomy after removal of a wedge (asterisk) brings about the rotation of the bone segment around the deformity axis, thereby completing the correction (A). When the deformity axis is along the convex side, an opening wedge osteotomy followed by wedge-shaped bone-grafting (double asterisks) is considered appropriate (B). When the axis is nearly parallel to the longitudinal bone axis, a rotational osteotomy (curved arrow) can be conducted in the osteotomy plane, which is perpendicular to the deformity axis (C). If the deformity axis is displaced from the bone, a closing or opening wedge osteotomy with shortening or lengthening is appropriate. The osteotomy planes are indicated by arrows.

This study included four distal humeral malunions (a cubitus varus deformity), ten diaphyseal malunions of the forearm, and eight malunited distal radial fractures. In the ten forearm malunions, the radius was malunited in four, the ulna was malunited in one, and both the radius and the ulna were malunited in five. The average age at the time of injury was 5.6 years for the patients with a cubitus varus deformity, twenty years for those with a forearm malunion, and forty-nine years for those with a malunion of the distal end of the radius. Initial treatment had consisted of closed reduction and cast immobilization in eighteen patients and open reduction and internal fixation in four patients.

At the time of initial presentation to our hospital, all patients demonstrated 5° to 45° of angular deformity of the bone on plain radiographs. Surgery was indicated because of a functional deficit in nineteen patients and an unsightly appearance in three patients. Nine of the ten patients with a forearm malunion had difficulty turning a doorknob and receiving a coin in the open palm because of restricted forearm rotation. The other patient (Case 7), who had malunited fractures of both bones of the forearm, reported recurrent anterior dislocation of the radial head accompanied by pain when he pronated the affected forearm. Three patients with a malunited forearm fracture (Cases 6, 11, and 12) and one patient with a malunited distal radial fracture (Case 20) had distal radioulnar joint subluxation. All of the patients with malunited distal radial fractures reported restricted range of wrist motion, moderate wrist pain, and decreased grip strength, and they experienced difficulty in using the affected hand in daily activities. One patient with cubitus varus (Case 1) could not perform simple activities, such as bringing food to the mouth, with the affected hand because of restricted elbow flexion. The other three patients with cubitus varus complained that the elbow had an unsightly appearance.

Simulation Technique

The affected and the contralateral limbs of all patients were scanned with use of a computed tomography scanner (LightSpeed Ultra 16; General Electric, Waukesha, Wisconsin), at a scan time of 0.5 sec, a scan pitch of 0.562:1, a tube current of 10 to 50 mA, and a tube voltage of 120 kV. Digital data from 0.625-mm slices were sent to a workstation (Precision Work-

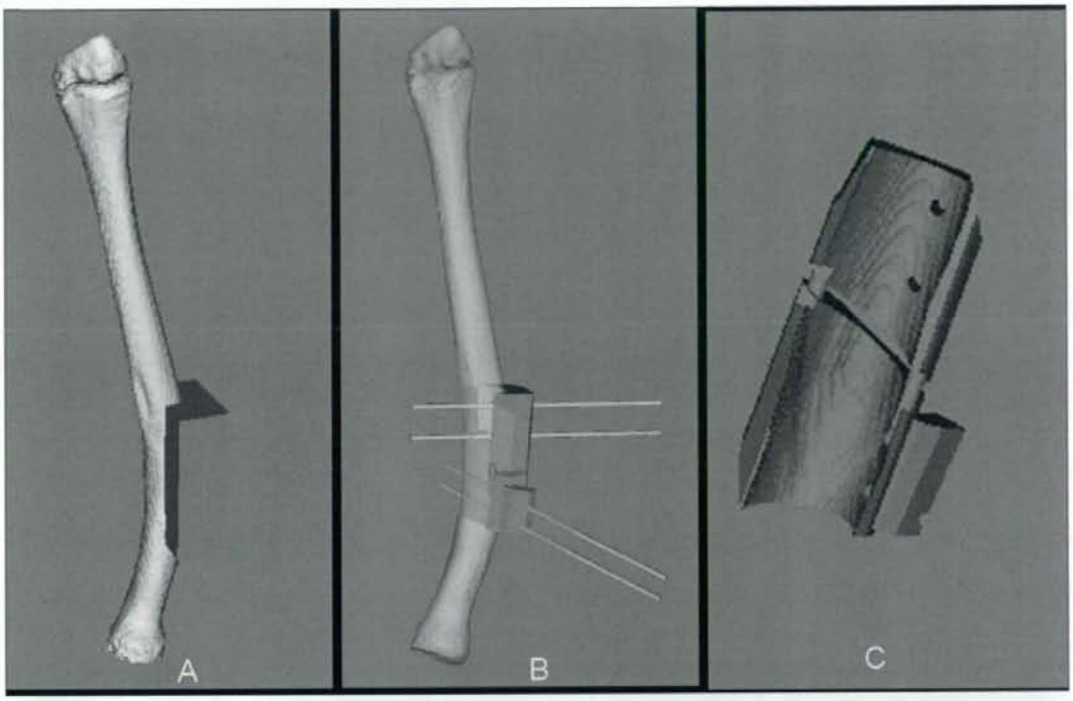

Fig. 3

Fig. 3 On the computer, a block of an appropriate size was placed on the bone surface that was to be exposed during surgery (A). The osteotomy plane, multiple cylinders, and the bone itself were subtracted from the block (B). The cylinders consist of two groups that have an angle of the deformity across the osteotomy plane. Finally, the computer design of the custom-made template was completed by shaping it (C).

Fig. 4 The osteotomy template was embodied as a real plastic model. These figures show the surgeon's side (A) and the bone-contacting side (B) of the template. (Reprinted, with permission, from: Murase T, Moritomo H, Sugamoto K, Yoshikawa H, Ogata K, Kawasaki K. [3D computer simulation for deformity correction of the limb]. Orthop Surg Traumatol. 2005;48:1055-60. Japanese.)

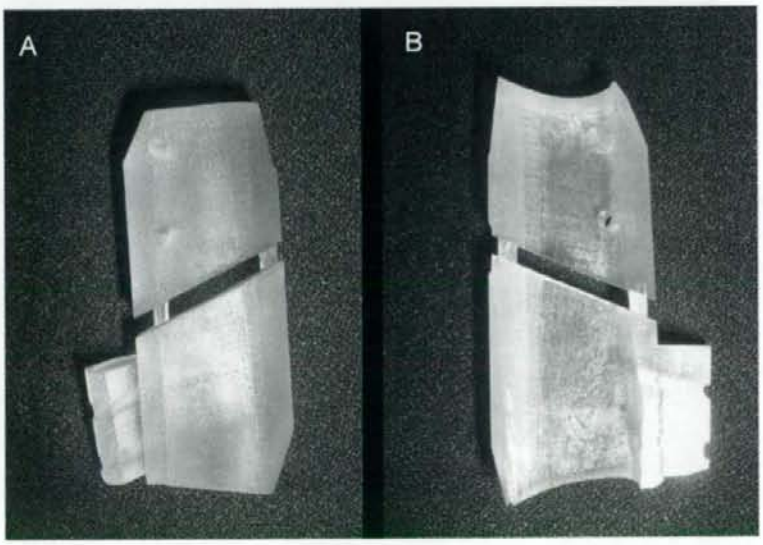

Fig. 4

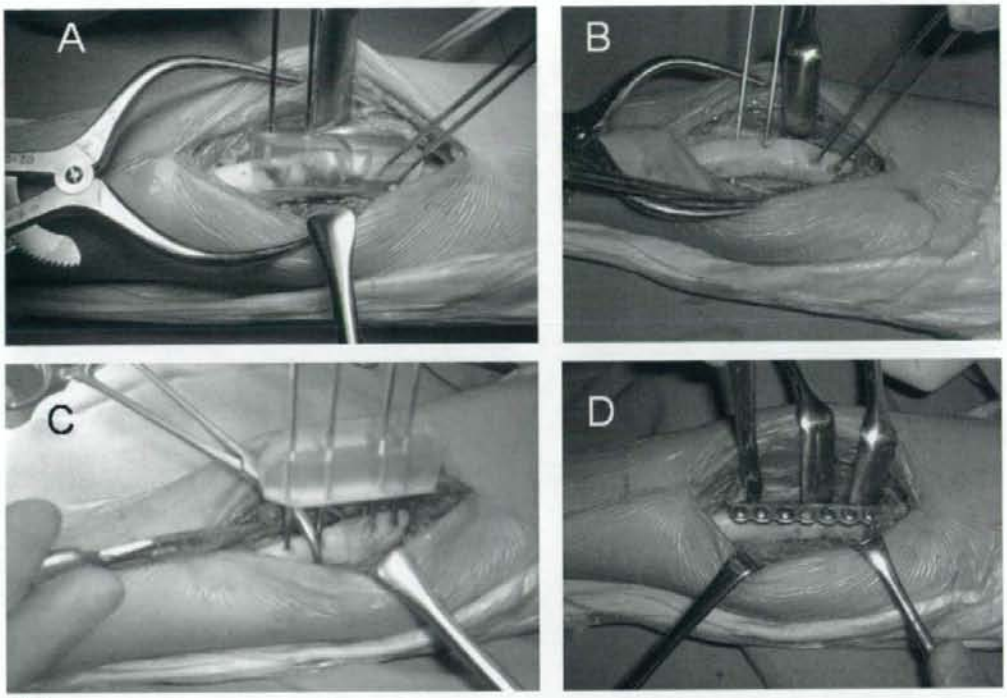

Fig. 5

Case 9. A fourteen-year-old boy with a malunited forearm fracture. The malunited radius was exposed through an anterior approach. The osteotomy template was fitted to the malunited site and fixed with Kirschner wires (A). The bone was divided through the cutting slit in the template, which was then removed (B). A reduction guide was used to maintain the Kirschner wires in a parallel position (C). Internal fixation was then accomplished with a plate and screws (D). (Reprinted, with permission, from: Murase T, Moritomo H, Sugamoto K, Yoshikawa H, Ogata K, Kawasaki K. [3D computer simulation for deformity correction of the limb]. Orthop Surg Traumatol. 2005;48:1055-60. Japanese.)

station 650; Dell, Round Rock, Texas). The malunited bones were segmented, and three-dimensional surface models were constructed by applying three-dimensional surface generation of the cortex of the bone[19] with use of the original computer program based on the Visualization Toolkit (Kitware, Clifton Park, New York). On the computer, the deformity of the affected bone was evaluated by superimposing[20] it with the goal model (e.g., the mirror image of a contralateral, normal bone), which can be further determined in terms of rotation around and translation along one unique axis, i.e., the three-dimensional deformity axis, with use of the screw displacement axis technique[21-23] (Fig. 1, *A*) (see Appendix for Videos 1 and 2). On the basis of the information obtained about the deformity axis, a corrective osteotomy was simulated[24,25] (Figs. 1, *B* and 2).

Design and Manufacturing of the Custom-Made Osteotomy Template

To reproduce the preoperative simulation during the actual surgery, we developed an operative method using a custom-made osteotomy template that was designed on the basis of a preoperative three-dimensional computer simulation with use of commercially available software (Magics RP; Materialise, Leuven, Belgium) and was embodied as a plastic model through rapid prototyping technology (Eden250; Objet Geometries, Rehovot, Israel, or Viper si2; 3D Systems, Rock Hill, South Carolina) with medical grade resin (Figs. 3 and 4). The custom-made osteotomy template has a shape that closely fits the bone surface and an osteotomy slit or slits and drill-holes that guide the insertion of the Kirschner wires. The slit guides the precise osteotomy cut; and the two sets of Kirschner wires, inserted through the drill-holes at an angle of the deformity, indicate that the reduction is completed when they become parallel to each other. A reduction guide to maintain the parallel position of the Kirschner wires is prepared preoperatively in the same manner as is the custom-made osteotomy template (see Appendix for Video 3).

Surgical Technique

During the procedure, the template was placed on the bone surface, the bone was osteotomized through a slit in the tem-

Fig. 6

Case 9. The preoperative anteroposterior radiograph of the forearm (A) shows anterior bowing of the radius. The postoperative anteroposterior (B) and lateral (C) radiographs show good anatomical correction. Note that the forearm is in a semipronated position preoperatively because of restricted forearm supination and is in a supinated position postoperatively. (Reprinted, with permission, from: Murase T, Moritomo H, Sugamoto K, Yoshikawa H, Ogata K, Kawasaki K. [3D computer simulation for deformity correction of the limb]. Orthop Surg Traumatol. 2005;48:1055-60. Japanese.)

plate, and the deformity was corrected as simulated preoperatively (Figs. 5 and 6). We were able to perform all osteotomies as preoperatively simulated. This was followed by internal fixation (plates and screws were used in twenty-four bones; Kirschner wires, including tension band wiring, were placed in two bones; and both methods of fixation were used in one bone). The template was fitted to the bone surface with reference to the characteristic configuration of the malunion and anatomical landmarks (e.g., the Lister tubercle, humeral condyles, and olecranon fossa). In patients with a malunited forearm fracture, the distance between the osteotomy site and the radial or ulnar styloid was calculated preoperatively on the computer and also served as a reference. A rotational osteotomy was performed on ten bones, a closing wedge osteotomy was done on five bones, and an opening wedge osteotomy with bone graft was performed on twelve bones. The amount of correction, which was the rotation around the three-dimensional deformity axis, ranged from 13° to 67°, with an average of 32°. In two rotational osteotomies, 3-mm and 2-mm shortenings along the deformity axis were required. In the other three rotational osteotomies, 2, 10, and 4-mm lengthenings with an interposition bone graft were required. These shortenings and lengthenings were performed to correct radioulnar discrepancies. The osteotomy template and the reduction guide were designed with consideration of these longitudinal adjustments. Open reduction of distal radioulnar joint subluxation in three patients with malunited forearm fractures (Cases 6, 11, and 12) and osteosynthesis of an ulnar styloid nonunion in one patient with a malunited distal radial fracture (Case 21) were combined with the corrective osteotomy.

The average time between the initial injury and the corrective osteotomy was thirteen years (range, two to twenty-seven years) for cubitus varus deformity, thirty months (range, six to 100 months) for malunited forearm fractures, and twelve